Published in final edited form as:

Structure. 2020 November 03; 28(11): 1225–1230.e3. doi:10.1016/j.str.2020.07.003.

Structural Insight into Binding of the ZZ Domain of HERC2 to Histone H3 and SUMO1

Jiuyang Liu[1,3], **Zhaoyu Xue**[2,3], **Yi Zhang**[1], **Kendra R. Vann**[1], **Xiaobing Shi**[2,*], **Tatiana G. Kutateladze**[1,4,*]

[1]Department of Pharmacology, University of Colorado School of Medicine, Aurora, CO 80045, USA

[2]Center for Epigenetics, Van Andel Research Institute, Grand Rapids, MI 49503, USA

[3]These authors contributed equally

[4]Lead Contact

SUMMARY

Human ubiquitin ligase HERC2, a component of the DNA repair machinery, has been linked to neurological diseases and cancer. Here, we show that the ZZ domain of HERC2 ($HERC2_{ZZ}$) binds to histone H3 tail and tolerates posttranslational modifications commonly present in H3. The crystal structure of the $HERC2_{ZZ}$:H3 complex provides the molecular basis for this interaction and highlights a critical role of the negatively charged site of $HERC2_{ZZ}$ in capturing of A1 of H3. NMR, mutagenesis, and fluorescence data reveal that $HERC2_{ZZ}$ binds to H3 and the N-terminal tail of SUMO1, a previously reported ligand of $HERC2_{ZZ}$, with comparable affinities. Like H3, the N-terminal tail of SUMO1 occupies the same negatively charged site of $HERC2_{ZZ}$ in the crystal structure of the complex, although in contrast to H3 it adopts an α-helical conformation. Our data suggest that $HERC2_{ZZ}$ may play a role in mediating the association of HERC2 with chromatin.

Graphical Abstract

*Correspondence: xiaobing.shi@vai.org (X.S.), tatiana.kutateladze@cuanschutz.edu (T.G.K.).

AUTHOR CONTRIBUTIONS

J.L., Z.X., Y.Z., and K.R.V. performed the experiments and, together with X.S. and T.G.K., analyzed the data. J.L. and T.G.K. wrote the manuscript with input from all authors.

SUPPLEMENTAL INFORMATION

Supplemental Information can be found online at https://doi.org/10.1016/j.str.2020.07.003.

DECLARATION OF INTERESTS

The authors declare no competing interests.

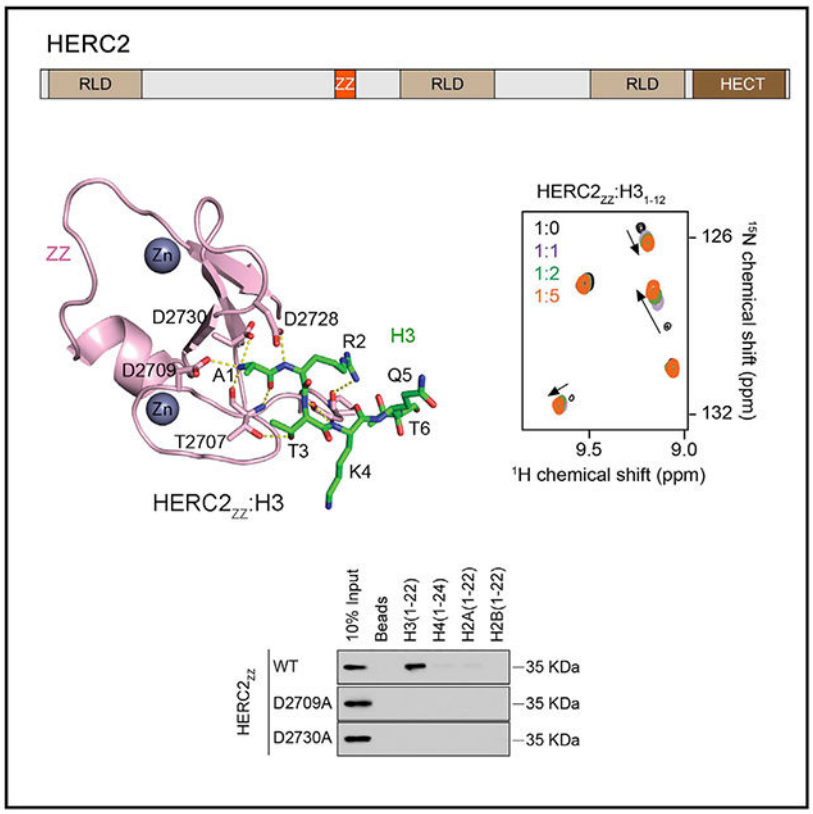

In Brief

Human ubiquitin ligase HERC2 is involved in cell response to various genotoxic stresses and is linked to neurological diseases and cancer. Liu et al. describe the molecular mechanism by which the ZZ domain of HERC2 binds to the N-terminal tails of histone H3 and SUMO1.

INTRODUCTION

The E3 ubiquitin protein ligase HERC2 is involved in DNA damage repair, immune stress response, and cell-cycle regulation. Mutations and aberrant activity of HERC2 are linked to neurological and autoimmune diseases, inflammation, and cancer (reviewed in Garcia-Cano et al., 2019). HERC2 is a large, 4,834-residue protein that contains the catalytic E3 ubiquitin ligase HECT domain, three RCC1-like domains (RLD) essential in DNA replication, and the ZZ-type zinc finger (Figure 1A). Following DNA damage, HERC2 undergoes SUMOylation and associates with another E3 ubiquitin ligase, RNF8, which ubiquitinates histone H2AX, recruiting repair factors to DNA damage foci and promoting DNA repair (Danielsen et al., 2012). It has been shown that the interaction between HERC2 and RNF8 requires the SUMO-binding activity of the ZZ domain of HERC2 (Danielsen et al., 2012), yet the molecular basis of this activity remains unclear.

Topologically, the ZZ domain belongs to a large family of RING fingers which also includes PHD and FYVE domains (Joazeiro and Weissman, 2000; Kutateladze, 2006; Musselman and Kutateladze, 2011). Although all RING fingers can be distinguished by two clusters

of zinc-coordinating cysteine/histidine residues, these domains bind distinct sets of ligands, including proteins, RNA, and phospholipids, and are implicated in different biological processes. Recent studies have shown that ZZ domains are capable of binding to either unmodified or acetylated histone H3 tails, whereas the ZZ domain of Mib1 has a scaffolding role (Itoh et al., 2003; Mi et al., 2018; Zhang et al., 2018b). The ZZ domain of yeast transcriptional adapter 2 interacts with an N-terminal extension of the GCN5 HAT domain, and the ZZ domain of CPEB1 was suggested to recognize proteins and/or RNA (Afroz et al., 2014; McMillan et al., 2015; Sun et al., 2018). In addition to being critical for cell nuclear signaling, some ZZ domains play important roles in cytoplasmic processes. For example, binding of the ZZ domain of p62 to arginylated substrates is necessary for selective autophagy (Zhang et al., 2018a, 2019). A wide array of the reported binding partners but limited structural and biochemical data make it difficult to predict selectivities of the ZZ domain family.

Here, we investigate binding of the ZZ domain of the E3 ubiquitin protein ligase HERC2 to histone H3 and SUMO1. The crystal structures of the complexes of $HERC2_{ZZ}$ with the N-terminal tails of H3 and SUMO1, along with analysis of NMR titration experiments, pull-down assays using histone peptides containing posttranslational modifications, measurements of binding affinities, and mutagenesis data provide the molecular basis underlying biological functions of $HERC2_{ZZ}$.

RESULTS AND DISCUSSION

We have previously reported that the ZZ domains of p300 and ZZZ3 ($p300_{ZZ}$ and $ZZZ3_{ZZ}$) recognize histone H3 tail (Mi et al., 2018; Zhang et al., 2018b). Comparison of the amino acid sequences of the ZZ domains from p300, ZZZ3, and HERC2 reveals that the three proteins exhibit ~48%–60% sequence similarity and ~35%–37% sequence identity (Figure S1). To determine whether the histone-binding function is conserved in the ZZ domain of HERC2 ($HERC2_{ZZ}$), we first tested GST-tagged $HERC2_{ZZ}$ in peptide pull-down assays (Figures 1B–1E). As shown in Figure 1B, GST-$HERC2_{ZZ}$ associated with the histone H3 peptide (residues 1–22 of H3) but did not recognize histone H4, H2A, and H2B peptides. Posttranslational modifications commonly present in the histone H3 tail, including methylated lysine 4 and lysine 9 (H3K4me and H3K9me), methylated arginine 2 (H3R2me), and acetylated lysine 4, lysine 9, lysine 14, and lysine 18 (H3K4ac/K9ac/K14ac/K18ac) did not affect binding of $HERC2_{ZZ}$ to H3 (Figures 1C–1E). To characterize this interaction in detail, we produced ^{15}N-labeled $HERC2_{ZZ}$ and recorded ^{1}H,^{15}N HSQC spectra of the protein while the histone H3 peptide (residues 1–12, $H3_{1-12}$) was added stepwise into the NMR sample. Addition of the peptide caused large chemical shift perturbations (CSPs) in $HERC2_{ZZ}$, which were in the intermediate exchange regime on the NMR timescale and indicated a tight binding (Figures 1F and S2). In agreement, a 15-μM binding affinity of $HERC2_{ZZ}$ for the $H3_{1-12}$ peptide was measured by a tryptophan fluorescence assay (Figures 1G and S3A).

To gain insight into the molecular mechanism by which $HERC2_{ZZ}$ recognizes histone H3, we generated a chimeric construct that contains the first six amino acids of H3 fused with the N terminus of $HERC2_{ZZ}$ ($H3_{1-6}$-$HERC_{ZZ}$), crystallized this construct, and determined

its crystal structure (Figures 2A and 2B; Table 1). Two $H3_{1-6}$-$HERC_{ZZ}$ molecules were observed per one asymmetric unit, with each $HERC_{ZZ}$ interacting with the $H3_{1-6}$ region from the other asymmetric unit molecules. In the complex, $HERC2_{ZZ}$ adopts a cross-braced structural topology, which is stabilized by two zinc-binding clusters, a twisted three-stranded anti-parallel β sheet, and an α helix (Figures 2A and 2B). The N-terminal residues of histone H3 (A1, R2, T3, and K4) make extensive intermolecular contacts with $HERC_{ZZ}$. A1 of histone H3 is bound in a highly negatively charged pocket, consisting of three aspartate residues of the protein, D2709, D2728, and D2730 (Figures 2C and S4A). The NH_3^+ group of A1 is captured through hydrogen bonds with the carboxyl groups of D2709 and D2730 and the backbone carbonyl of T2707. The backbone of histone H3 is restrained by several hydrogen bonds formed between the carbonyl group of A1, the amides of R2, T3, and K4 of H3 and the ZZ's backbone amide of T2707, the carboxyl group of D2728, and the carbonyl of G2705, respectively (Figures 2C and S4A). The side chain guanidino moiety of R2 of H3 donates a hydrogen bond to the backbone carbonyl of P2704, and another hydrogen bond is formed between hydroxyl groups of T3 of H3 and T2707 of ZZ. The side chain amino group of K4 is solvent exposed, which helps to explain that methylation or acetylation of H3K4 have no effect on the interaction of $HERC2_{ZZ}$ with H3.

We next assessed the contribution of the interfacial residues in the $HERC2_{ZZ}$:H3 complex formation. Pull-down experiments using the H3 peptide (residues 3–22 of H3) lacking the first two amino acids, A1 and R2, showed that binding of $HERC2_{ZZ}$ was substantially decreased (Figure 2D). These data indicate an important role of the A1 and R2 residues of H3 in the interaction. We note that a free alanine amino acid was insufficient to form the complex with $HERC2_{ZZ}$, because no CSPs in $HERC2_{ZZ}$ were observed upon addition of a 50-fold excess of alanine in the NMR titration experiment (Figure S5). Binding of $HERC2_{ZZ}$ to the AGSGSG peptide was noticeably reduced (K_d = 374 μM), which pointed to a contribution of the hydrogen bonding contacts involving the side chains of the H3 residues, R2 and T3, in binding energetics (Figure S6). However, mutation of a single aspartate in $HERC2_{ZZ}$, either D2709 or D2730 to alanine, essentially eliminated binding to H3, as seen in pull-down assays and NMR titration experiments (Figures 2E and 2F). Western blot analysis of FLAG IPs in HEK293T cells expressing H3-FLAG and $HERC2_{2600-4834}$ (residues 2,600–4,834 of HERC2), a large construct which encompasses the C-terminal half of HERC2, showed that binding of $HERC2_{2600-4834}$ to chromatin is also decreased when D2709 and D2730 are substituted with alanine (Figure 2G).

$HERC2_{ZZ}$ has previously been shown to associate with SUMO1 and facilitate the SUMOylation-dependent response to DNA damage (Danielsen et al., 2012). To elucidate the molecular basis of this association, we examined binding of $HERC2_{ZZ}$ to the full-length SUMO1 protein ($SUMO1_{FL}$) and the $SUMO1_{1-6}$ peptide (residues 1–6 of SUMO1, SDQEAK) by NMR, tryptophan fluorescence, and X-ray crystallography. Titration of unlabeled $SUMO1_{FL}$ into the ^{15}N-labeled $HERC2_{ZZ}$ led to substantial CSPs in the intermediate exchange regime on the NMR time-scale, confirming the direct and tight interaction (Figures 3A and S7). Almost identical CSPs in $HERC2_{ZZ}$ were induced by the $SUMO1_{1-6}$ peptide or the $SUMO1_{FL}$ protein, indicating that the first six N-terminal residues of SUMO1 interact with $HERC2_{ZZ}$ (Figures 3A and S8). A reverse titration of unlabeled $HERC2_{ZZ}$ into the ^{15}N-labeled $SUMO1_{FL}$ protein also caused CSPs, further confirming

the direct binding of the two proteins (Figure 3B). The dissociation constant (K_d) for the interaction of $HERC2_{ZZ}$ with the $SUMO1_{1-6}$ peptide was found to be 8 μM, as measured by tryptophan fluorescence (Figures 3C and S3B). This value was in agreement with a 3-μM binding affinity of $HERC2_{ZZ}$ toward $SUMO1_{FL}$, measured previously by ITC (Danielsen et al., 2012).

To define the molecular basis for the association of $HERC2_{ZZ}$ with SUMO1, we produced a construct fusing $SUMO1_{1-6}$ with $HERC2_{ZZ}$, crystallized it, and obtained the crystal structure of the complex. Interestingly, we found that SUMO1 occupies the same binding site of $HERC2_{ZZ}$ as histone H3 (Figures 2A–2C and 3D–3F). The carboxyl groups of D2709 and D2730 and the backbone carbonyl of T2707 of $HERC2_{ZZ}$ form hydrogen bonds with the NH_3^+ group of S1. The backbone amides of D2 and Q3 of SUMO1 are restrained through formation of hydrogen bonds with the D2728 carboxyl group and the carbonyl of G2705, respectively. In addition, the side chain hydroxyl group of S1 is hydrogen bonded to the carboxyl group of D2709, and another hydrogen bond is formed between the side chain carboxyl group of D2 and the guanidino group of R2720. Substitution of D2709 or D2730 with alanine in $HERC2_{ZZ}$ abolished its interaction with either the $SUMO1_{FL}$ protein or the $SUMO1_{1-6}$ peptide, underscoring the critical role of the direct contacts of these aspartate residues with the S1 residue of SUMO1 (Figures 3G, 3H, and S9).

Despite the differences in the amino acid sequences of SUMO1 (SDQEAK) and H3 (ARTKQT), both ligands occupy the same binding site of $HERC2_{ZZ}$, although in the complex SUMO1 adopts an α-helical conformation, whereas histone H3 is bound as a random coil. The most striking similarity in the binding mechanisms is the way the first residues in H3 (A1) and SUMO1 (S1) are recognized by $HERC2_{ZZ}$. The NH_3^+ group of either A1 or S1 donates three hydrogen bonds to D2709, D2730, and T2707, whereas the backbone carbonyl of A1/S1 is hydrogen bonded to T2707. Furthermore, in both complexes the backbone amide of the second residue (R2 in H3 and D2 in SUMO1), forms a hydrogen bond with D2728. However, the patterns of intermolecular contacts for the rest of the ligands' residues are distinctly different.

What are the biological consequences of the H3 and SUMO1 recognition by $HERC2_{ZZ}$? The catalytic HECT domain of HERC2 undergoes SUMOylation in response to double-strand break of DNA (Danielsen et al., 2012), and intra- or intermolecular SUMO binding by $HERC2_{ZZ}$ may play a role in mediating conformational changes, DNA-binding activity, chromatin localization, and catalytic function of HERC2 (Figure 3I). A similar SUMO1-dependent regulation has been proposed for the DNA repair enzyme thymine-DNA glycosylase (Eilebrecht et al., 2010; Geiss-Friedlander and Melchior, 2007; Mohan et al., 2007; Smet-Nocca et al., 2011). Since $HERC2_{ZZ}$ exhibits strong histone H3- and SUMO1-binding activities, it will be interesting in future studies to explore the interplay between these functions of $HERC2_{ZZ}$ and test several ideas—for example, whether SUMOylation of the HECT domain of HERC2 interferes with binding of $HERC2_{ZZ}$ to H3 in cells, and whether $HERC2_{ZZ}$ contributes to the association with chromatin only in the absence of HERC2 SUMOylation. It will also be important to determine whether the intra-/intermolecular interaction between $HERC2_{ZZ}$ and the SUMO covalently attached to the HECT domain of HERC2 can induce a conformational change and, if yes, what is the

biological significance of this change? Finally, future studies are also needed to establish the role of posttranslational modifications of SUMO1, including N-terminal acetylation and phosphorylation of S1, in mediating the SUMO1-, HERC2-, and RNF8-dependent response to DSBs (Danielsen et al., 2012; Matic et al., 2008).

STAR★METHODS

RESOURCE AVAILABILITY

Lead Contact—Further information and requests for resources and reagents should be directed to and will be fulfilled by the Lead Contact, Tatiana Kutateladze (tatiana.kutateladze@cuanschutz.edu).

Materials Availability—All reagents generated in this study will be made available on request, but we may require a payment and/or a completed Materials Transfer Agreement if there is potential for commercial application.

Data and Code Availability—Coordinates and structure factors have been deposited in the Protein Data Bank under ID codes 6WW3 and 6WW4.

EXPERIMENTAL MODEL AND SUBJECT DETAILS

$HERC2_{ZZ}$ was expressed in BL21 (DE3) RIL in LB or minimal media supplemented with $^{15}NH_4Cl$ and 0.05 mM $ZnCl_2$. Protein expression was induced with 0.2 mM IPTG for 20 h at 16°C.

HEK293T (ATCC ® CRL-3216, RRID: CVCL_0063) the human female cells were maintained in DMEM supplemented with 10% FBS, 2mM L-glutamine and 100 U/mL penicillin/streptomycin, 37°C, 5% CO2.

METHOD DETAILS

Protein Expression and Purification—Human $HERC2_{ZZ}$ (aa 2702-2755), H3-$HERC2_{ZZ}$ (aa 1-6 of histone H3, aa 2702-2755 of $HERC2_{ZZ}$) and SUMO1-$HERC2_{ZZ}$ (aa 1-6 of SUMO1, aa 2702-2755 of $HERC2_{ZZ}$) constructs were cloned into pCIOX vectors with N-terminal His_{8x}-SUMO tag and Ulp1 cleavage site. An extra tryptophan residue was introduced at the C terminal of $HERC2_{ZZ}$ in order to quantify the protein and perform tryptophan fluorescence assays. The human SUMO1 protein was cloned into a pDEST-15 vector with N-terminal GST tag and TEV cleavage site. Proteins were expressed in BL21 (DE3) RIL in LB or minimal media supplemented with $^{15}NH_4Cl$ and 0.05 mM $ZnCl_2$. Protein expression was induced with 0.2 mM IPTG for 20 h at 16 °C. The His_{8x}-SUMO tagged proteins were purified on Ni-NTA beads (Qiagen) in 50 mM Tris-HCl (pH 7.5) buffer, supplemented with 500 mM NaCl, 1 mM phenylmethanesulfonyl fluoride and 10 mM β-mercaptoethanol. The SUMO tag was cleaved overnight at 4 °C with Ulp1 protease. The GST-tagged proteins were purified on glutathione Sepharose 4B beads (GE Healthcare) in 20 mM Tris-HCl (pH 7.5) buffer, supplemented with 200 mM NaCl and 5 mM DTT. The GST tag was cleaved overnight at 4 °C with TEV protease. Proteins were further purified by size exclusion chromatography and concentrated in Millipore concentrators. All mutants

were generated by site-directed mutagenesis using the Stratagene QuikChange mutagenesis protocol, then grown and purified as wild-type proteins.

Peptide Pull-down Assays—Peptide pull-down assays were performed as described previously (Mi et al., 2018). In brief, 1 μg of biotinylated at their C-termini histone peptides with or without different modifications were incubated with 1–2 μg of GST-fused $HERC2_{ZZ}$ in binding buffer (50 mM Tris–HCl 7.5, 300 mM NaCl, 0.1% NP-40, and 1 mM phenylmethanesulfonyl fluoride) overnight with rotation at 4 °C. Streptavidin magnetic beads (Pierce) were added to the mixture, and the mixture was incubated for 1 h with rotation at 4 °C. The beads were then washed three times with buffer (50 mM Tris–HCl 7.5, 300 mM NaCl, and 0.1% NP-40) and analyzed using SDS-PAGE and western blotting.

NMR Experiments—NMR experiments were carried out at 298K on a Varian INOVA 600 spectrometer as described (Gatchalian et al., 2017). NMR samples contained 0.1 mM uniformly ^{15}N-labeled WT, mutated $HERC2_{ZZ}$ or SUMO1 in 20 mM Tris (pH 6.8) buffer supplemented with 100 mM NaCl, 2-5 mM DTT, and 10% D_2O. Binding was characterized by monitoring chemical shift changes in the proteins induced by H3, SUMO1 peptides (synthesized by SynPeptide) or unlabeled $HERC2_{ZZ}$. All peptides used in NMR experiments are not biotinylated and not acetylated.

X-Ray Crystallography—The purified H3-$HERC2_{ZZ}$ and SUMO1-$HERC2_{ZZ}$ were concentrated to 3~5 mg/ml in a buffer containing 20 mM Tris (pH 8.0), 200 mM NaCl, 5 mM DTT. The H3-$HERC2_{ZZ}$ crystals were obtained at 25 °C by sitting drop vapor diffusion in 0.1 M ammonium acetate, 0.1 M Bis-Tris, pH 5.5 and 17% PEG 10000. The SUMO1-$HERC2_{ZZ}$ crystals were obtained at 25 °C by sitting drop vapor diffusion in 0.2 M ammonium chloride, 0.1 M Tris, pH 8.0 and 20% PEG 6000. Crystals were cryoprotected with the addition of 25% glycerol before flash-frozen in liquid nitrogen and the X-ray diffraction data were collected at the Advanced Light Source beamline 4.2.2 administrated by the Molecular Biology Consortium or on the Rigaku Micromax 007 high-frequency microfocus X-ray generator in CU Anschutz X-ray crystallography core facility. HKL2000 was used for indexing, scaling, and data reduction (Otwinowski and Minor, 1997). The structures were determined using Molrep program in CCP4 with $P300_{ZZ}$ (PDB code: 6DS6) as the search model (Zhang et al., 2018b). Model building was performed using Coot (Emsley et al., 2010), and the structure was refined using Phenix Refine (Adams et al., 2010). The X-ray diffraction and structure refinement statistics are summarized in Table 1.

Tryptophan Fluorescence—Spectra were recorded at 25 °C on a Fluoromax-3 spectrofluorometer (HORIBA). The samples containing 5 μM $HERC2_{ZZ}$ fragment (aa 2702-2755) and progressively increasing concentrations of the $H3_{1-12}$ and $SUMO1_{1-6}$ (without biotin and not acetylated at their N-termini) peptides were excited at 295 nm. Experiments were performed in buffer containing 20 mM Tris-HCl (pH 6.8), 150 mM NaCl, and 2 mM DTT. Emission spectra were recorded over a range of wavelengths between 330 nm and 360 nm with a 0.5 nm step size and a 1 s integration time and averaged over 3 scans. The K_d values were determined using a nonlinear least-squares analysis and the equation:

$$\Delta I = \Delta I_{max} \frac{\left(([L]+[P]+K_d) - \sqrt{([L]+[P]+K_d)^2 - 4[P][L]}\right)}{2[P]}$$

where [L] is the concentration of the peptide, [P] is the concentration of $HERC2_{ZZ}$. ΔI represents the change of signal intensity, ΔI is the observed change of signal intensity, and ΔI_{max} is the difference in signal intensity of the free and bound states of the $HERC2_{ZZ}$. The K_d value was averaged over three separate experiments, with error calculated as the standard deviation between the runs.

Co-immunoprecipitation—For co-immunoprecipitations (Co-IPs), HEK293T cells in 10 cm dishes were transiently transfected with pcDNA-H3-FLAG and pcDNA plasmids encoding the wild-type (WT) HERC2 (aa 2600-4834) or the indicated ZZ domain point mutants. 48 hrs after transfections, the cells were collected, resuspended in cold cell lysis buffer (50 mM Tris-HCl pH7.4, 250 mM NaCl, 0.5% Triton X100, 10% glycerol, 1 mM DTT, 1mM PMSF, and 1x protease inhibitors) and incubated on ice for 30 min. Cells were then briefly sonicated, centrifuged at 13,000 rpm for 10 min to collect the supernatants. Cell lysates were incubated with the ANTI-FLAG M2 beads (Sigma-Aldrich) at 4°C for 4 hrs, subsequently the beads were washed 5 times with 1 ml of cold cell lysis buffer and boiled in SDS sample buffer for SDS-PAGE electrophoresis. For Western blot analysis, the following antibodies were used: anti-HERC2 (Abcam, Ab85832, 1:1000), FLAG (Sigma, F3165, 1:5000).

QUANTIFICATION AND STATISTICAL ANALYSIS

The crystal structures of $HERC2_{ZZ}$ in complex with $H3_{1-6}$ and $SUMO1_{1-6}$ tails were determined using materials and softwares listed in the Key Resources Table. Statistics generated from X-ray crystallography data processing, refinement, and structure validation are displayed in Table 1.

Tryptophan fluorescence assays shown in Figures 1G, 3C, S3, and S6 were performed in three independent replicates. The K_d values were determined by a nonlinear least-squares analysis using KaleidaGraph 4.5 (Synergy Software) and calculated as means ± SD.

Supplementary Material

Refer to Web version on PubMed Central for supplementary material.

ACKNOWLEDGMENTS

We thank JaeWoo Ahn for help with experiments. This work was supported by grants from NIH GM135671, CA252707, and HL151334 (to T.G.K.) and CA204020 (to X.S.). X.S. is a Leukemia & Lymphoma Society Career Development Program Scholar. Y.Z. is supported by NIH K99CA241301.

REFERENCES

Adams PD, Afonine PV, Bunkoczi G, Chen VB, Davis IW, Echols N, Headd JJ, Hung LW, Kapral GJ, Grosse-Kunstleve RW, et al. (2010). PHENIX: a comprehensive Python-based system for

macromolecular structure solution. Acta Crystallogr. D Biol. Crystallogr 66, 213–221. [PubMed: 20124702]

Afroz T, Skrisovska L, Belloc E, Guillen-Boixet J, Mendez R, and Allain FH (2014).A fly trap mechanism provides sequence-specific RNA recognition by CPEB proteins. Genes Dev. 28, 1498–1514. [PubMed: 24990967]

Danielsen JR, Povlsen LK, Villumsen BH, Streicher W, Nilsson J, Wikstrom M, Bekker-Jensen S, and Mailand N (2012). DNA damage-inducible SUMOylation of HERC2 promotes RNF8 binding via a novel SUMO-binding Zinc finger. J. Cell Biol 197, 179–187. [PubMed: 22508508]

Eilebrecht S, Smet-Nocca C, Wieruszeski JM, and Benecke A (2010). SUMO-1 possesses DNA binding activity. BMC Res. Notes 3, 146.

Emsley P, Lohkamp B, Scott WG, and Cowtan K (2010). Features and development of Coot. Acta Crystallogr. D Biol. Crystallogr 66, 486–501. [PubMed: 20383002]

Garcia-Cano J, Martinez-Martinez A, Sala-Gaston J, Pedrazza L, and Rosa JL (2019). HERCing: structural and functional relevance of the large HERC ubiquitin ligases. Front. Physiol 10, 1014. [PubMed: 31447701]

Gatchalian J, Wang X, Ikebe J, Cox KL, Tencer AH, Zhang Y, Burge NL, Di L, Gibson MD, Musselman CA, et al. (2017). Accessibility of the histone H3 tail in the nucleosome for binding of paired readers. Nat. Commun 3, 1489.

Geiss-Friedlander R, and Melchior F (2007). Concepts in sumoylation: a decade on. Nat. Rev. Mol. Cell Biol 8, 947–956. [PubMed: 18000527]

Huang H, Sabari BR, Garcia BA, Allis CD, and Zhao YM (2014). SnapShot: histone modifications. Cell 159, 458–458.e1. [PubMed: 25303536]

Itoh M, Kim CH, Palardy G, Oda T, Jiang YJ, Maust D, Yeo SY, Lorick K, Wright GJ, Ariza-McNaughton L, et al. (2003). Mind bomb is a ubiquitin ligase that is essential for efficient activation of Notch signaling by Delta. Dev. Cell 4, 67–82. [PubMed: 12530964]

Joazeiro CA, and Weissman AM (2000). RING finger proteins: mediators of ubiquitin ligase activity. Cell 102, 549–552. [PubMed: 11007473]

Kutateladze TG (2006). Phosphatidylinositol 3-phosphate recognition and membrane docking by the FYVE domain. Biochim. Biophys. Acta 1761, 868–877. [PubMed: 16644267]

Matic I, Macek B, Hilger M, Walther TC, and Mann M (2008). Phosphorylation of SUMO-1 occurs in vivo and is conserved through evolution. J. Proteome Res 7, 4050–4057. [PubMed: 18707152]

McMillan BJ, Schnute B, Ohlenhard N, Zimmerman B, Miles L, Beglova N, Klein T, and Blacklow SC (2015). A tail of two sites: a bipartite mechanism for recognition of notch ligands by mind bomb E3 ligases. Mol. Cell 57, 912–924. [PubMed: 25747658]

Mi W, Zhang Y, Lyu J, Wang X, Tong Q, Peng D, Xue Y, Tencer AH, Wen H, Li W, et al. (2018). The ZZ-type zinc finger of ZZZ3 modulates the ATAC complex-mediated histone acetylation and gene activation. Nat. Commun 9, 3759. [PubMed: 30217978]

Mohan RD, Rao A, Gagliardi J, and Tini M (2007). SUMO-1-dependent allosteric regulation of thymine DNA glycosylase alters subnuclear localization and CBP/p300 recruitment. Mol. Cell. Biol 27, 229–243. [PubMed: 17060459]

Musselman CA, and Kutateladze TG (2011). Handpicking epigenetic marks with PHD fingers. Nucleic Acids Res. 39, 9061–9071. [PubMed: 21813457]

Otwinowski Z, and Minor W (1997). Processing of X-ray diffraction data collected in oscillation mode. Methods Enzymol. 276, 307–326. [PubMed: 27754618]

Smet-Nocca C, Wieruszeski JM, Leger H, Eilebrecht S, and Benecke A (2011). SUMO-1 regulates the conformational dynamics of thymine-DNA glycosylase regulatory domain and competes with its DNA binding activity. BMC Biochem. 12, 4. [PubMed: 21284855]

Sun J, Paduch M, Kim SA, Kramer RM, Barrios AF, Lu V, Luke J, Usatyuk S, Kossiakoff AA, and Tan S (2018). Structural basis for activation of SAGA histone acetyltransferase Gcn5 by partner subunit Ada2. Proc. Natl. Acad. Sci. U S A 115, 10010–10015. [PubMed: 30224453]

Zhang Y, Mun SR, Linares JF, Ahn J, Towers CG, Ji CH, Fitzwalter BE, Holden MR, Mi W, Shi X, et al. (2018a). ZZ-dependent regulation of p62/SQSTM1 in autophagy. Nat. Commun 9, 4373. [PubMed: 30349045]

Zhang Y, Mun SR, Linares JF, Towers CG, Thorburn A, Diaz-Meco MT, Kwon YT, and Kutateladze TG (2019). Mechanistic insight into the regulation of SQSTM1/p62. Autophagy, 1–3.

Zhang Y, Xue Y, Shi J, Ahn J, Mi W, Ali M, Wang X, Klein BJ, Wen H, Li W, et al. (2018b). The ZZ domain of p300 mediates specificity of the adjacent HAT domain for histone H3. Nat. Struct. Mol. Biol 25, 841–849. [PubMed: 30150647]

Highlights

- The ZZ domain of HERC2 ($HERC2_{ZZ}$) recognizes histone H3
- Binding to H3 is essential for the association of HERC2 with chromatin
- Ala1 of H3 is caged by aspartate residues of $HERC2_{ZZ}$
- The N-terminal tails of SUMO1 and H3 are bound in the same site of $HERC2_{ZZ}$

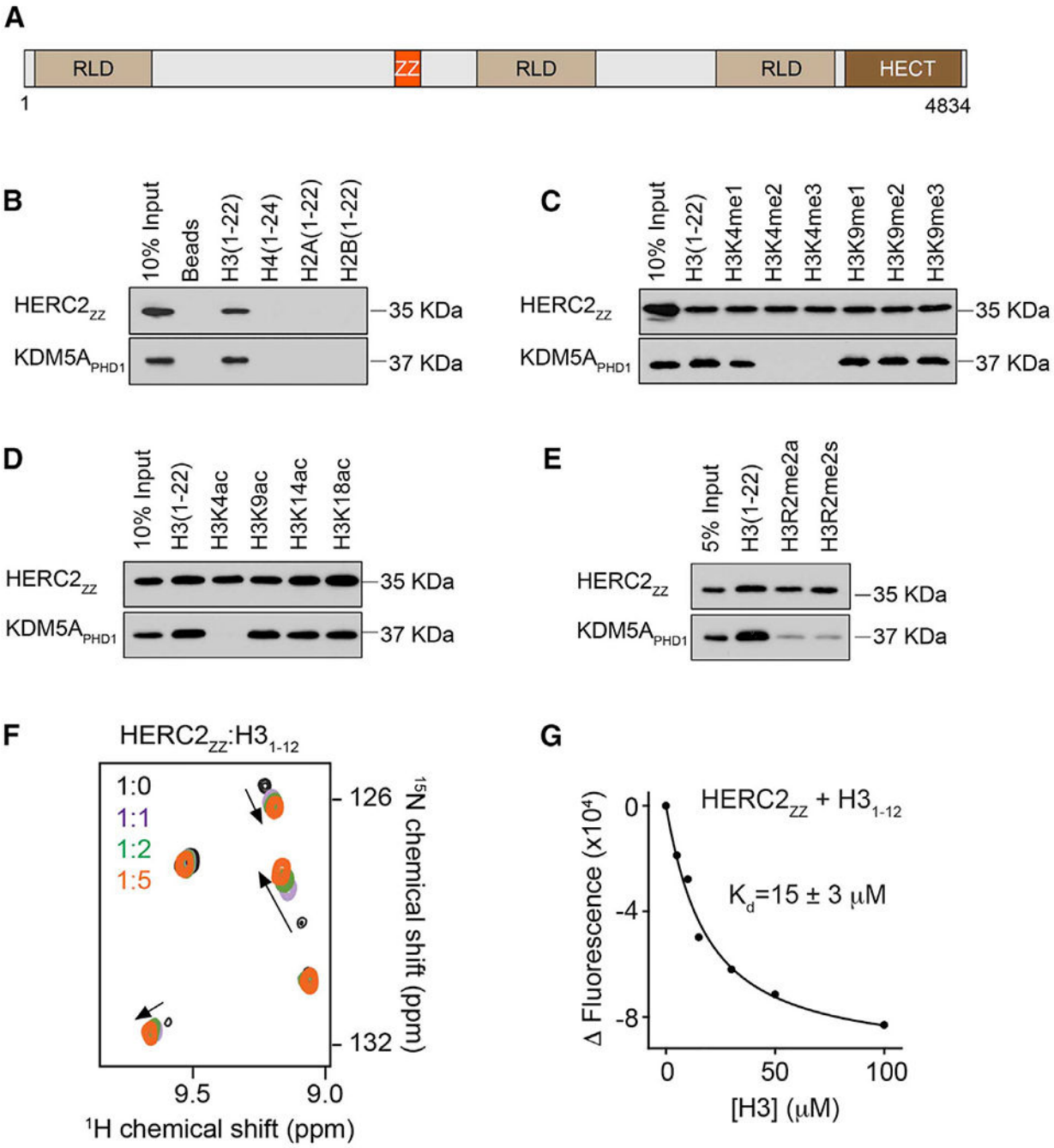

Figure 1. HERC2$_{ZZ}$ Binds to Histone H3

(A) A schematic representation of HERC2 with the ZZ domain highlighted in orange. (B–E) Peptide pull-down assays of HERC2$_{ZZ}$ with indicated histone peptides. All peptides are biotinylated at their C termini. The H2A and H4 peptides are acetylated at their N termini, and the H3 and H2B peptides have the free NH_3^+ group at their N termini, as in Huang et al. (2014). The PHD1 finger of KDM5A is used as control.

(F) Overlay of $^{1}H,^{15}N$ HSQC spectra of ^{15}N-labeled $HERC2_{ZZ}$ collected before (black) and after the addition of the $H3_{1-12}$ peptide. Spectra are color coded according to the protein-peptide molar ratio as indicated.

(G) Representative binding curves used to determine the K_d values by tryptophan fluorescence. The K_d value was averaged over three separate experiments, with error calculated as the standard deviation between the runs.

See also Figures S1–S3.

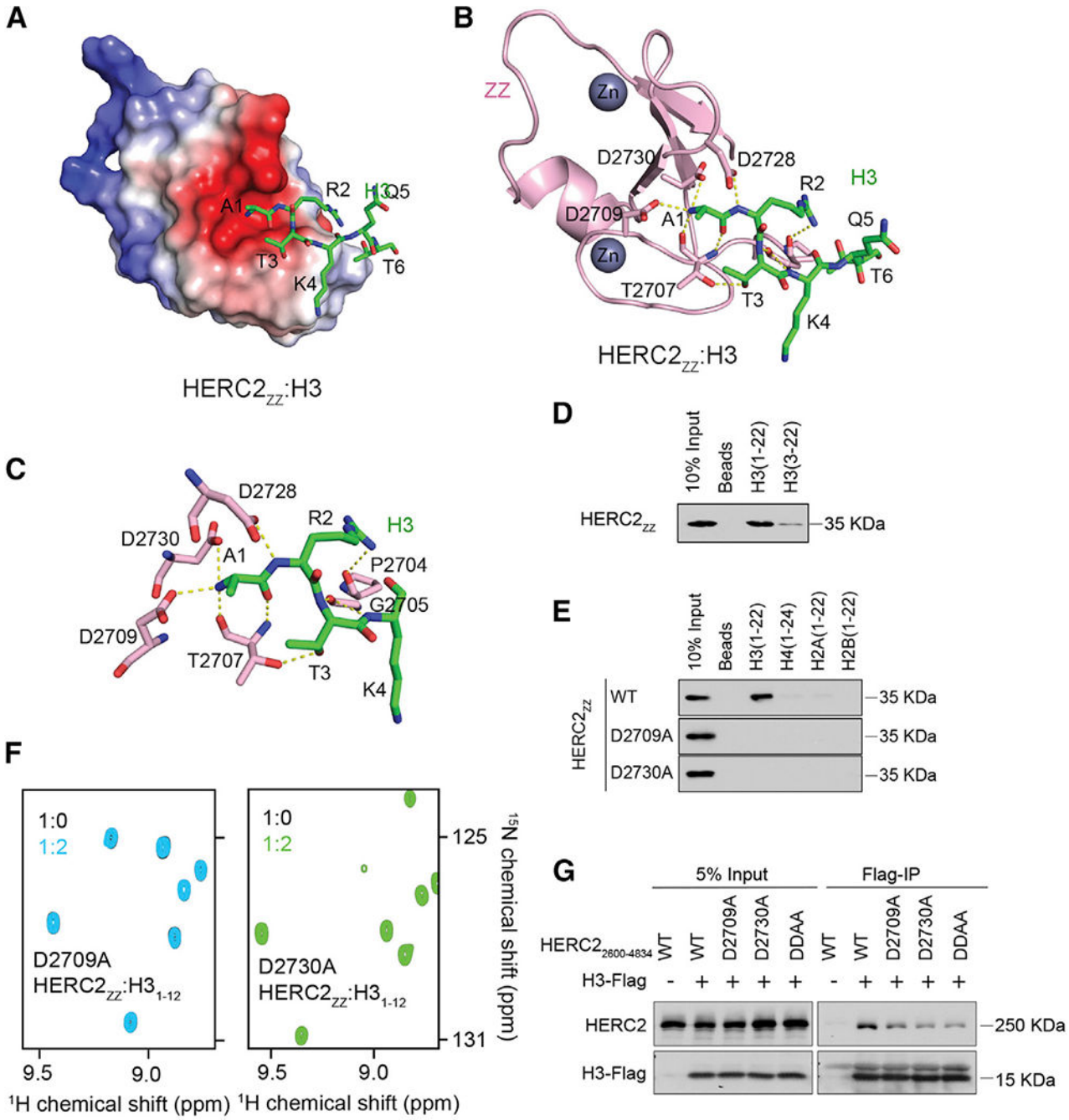

Figure 2. Structural Basis for the Recognition of H3 by HERC2ZZ

(A) The crystal structure of the HERC2ZZ:H3$_{1-6}$ complex. Electrostatic surface potential of HERC2ZZ is colored blue and red for positive and negative charges, respectively. The bound H3 is shown in green sticks.

(B) HERC2ZZ is shown in a ribbon diagram (pink), and H3 is shown in green sticks. The zinc atoms are shown as gray spheres, and hydrogen bonds are depicted as yellow dashed lines.

(C) A zoom-in view of the H3-binding site of HERC2ZZ.

(D and E) Peptide pull-down assays of wild-type (WT) and mutated $HERC2_{ZZ}$ with indicated histone peptides. All peptides are biotinylated at their C termini. The H2A and H4 peptides are acetylated at their N termini, and the H3 and H2B peptides have the free NH_3^+ group at their N termini.

(F) Overlay of ^{1}H,^{15}N HSQC spectra of the ^{15}N-labeled D2709A and D2730A mutants of $HERC2_{ZZ}$ collected before (black) and after (blue and green) addition of the $H3_{1-12}$ peptide. Spectra are color coded according to the protein-peptide molar ratio as indicated.

(G) Western blots of FLAG IPs in cells expressing H3-FLAG and the WT HERC2 (amino acids 2,600–4,834) or the indicated ZZ domain point mutants. DDAA, double mutations of D2709A/D2730A.

See also Figures S4–S6.

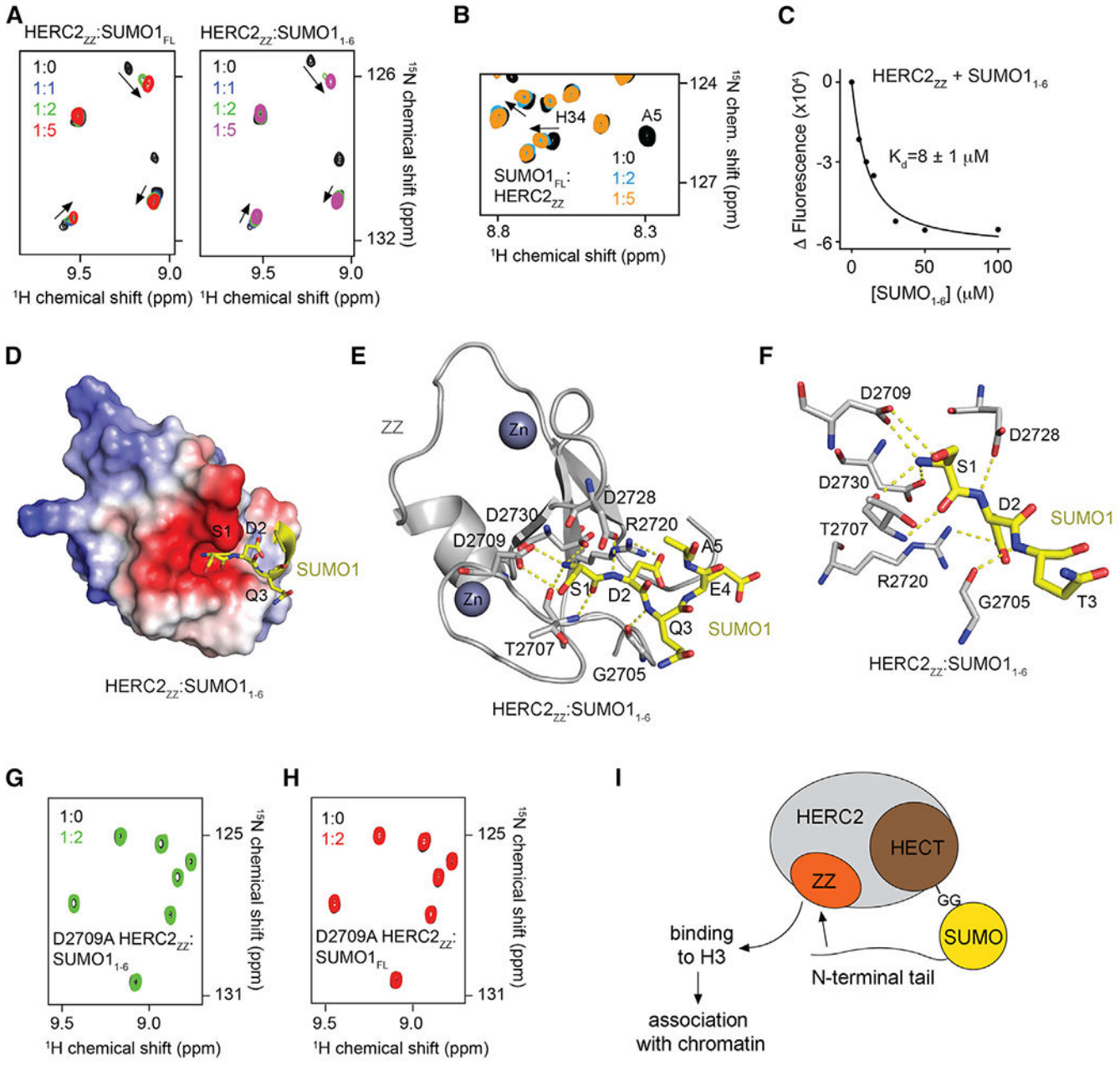

Figure 3. Molecular Mechanism of the Association of HERC2$_{ZZ}$ with SUMO1

(A) Overlays of ^{1}H,^{15}N HSQC spectra of ^{15}N-labeled HERC2$_{ZZ}$ collected before (black) and after the addition of the full-length SUMO1$_{FL}$ protein (left) or the SUMO1$_{1-6}$ peptide (right). Spectra are color coded according to the protein-ligand molar ratio as indicated.

(B) Overlay of ^{1}H,^{15}N HSQC spectra of the ^{15}N-labeled full-length SUMO1$_{FL}$ protein collected before (black) and after the addition of unlabeled HERC2$_{ZZ}$. Spectra are color coded according to the protein-ligand molar ratio as indicated.

(C) Representative binding curves used to determine the K_d values by tryptophan fluorescence. The K_d value was averaged over three separate experiments, with error calculated as the standard deviation between the runs.

(D) The crystal structure of the $HERC2_{ZZ}$:$SUMO1_{1-6}$ complex. Electrostatic surface potential of $HERC2_{ZZ}$ is colored blue and red for positive and negative charges, respectively. The bound SUMO1 is yellow.

(E) $HERC2_{ZZ}$ is shown in a ribbon diagram (gray), and SUMO1 is shown in yellow sticks. The zinc atoms are shown as gray spheres, and hydrogen bonds are depicted as yellow dashed lines.

(F) A zoom-in view of the SUMO1-binding site of $HERC2_{ZZ}$.

(G and H) Overlays of ^{1}H,^{15}N HSQC spectra of the ^{15}N-labeled D2709A and D2730A mutants of $HERC2_{ZZ}$ collected before (black) and after the addition of the $SUMO1_{1-6}$ peptide (green) (G) or the full-length $SUMO1_{FL}$ protein (red) (H). Spectra are color coded according to the protein-ligand molar ratio as indicated.

(I) A model of the interplay between H3- and SUMO-binding activities of $HERC2_{ZZ}$. The catalytic HECT domain (brown) of HERC2 is covalently linked to SUMO (via a GG motif that becomes exposed after SUMO1 is proteolytically processed at its C terminus) (yellow). The ZZ domain (orange) of HERC2 is capable of binding to the N-terminal tails of SUMO and H3.

See also Figures S3, S4, and S7–S9.

KEY RESOURCES TABLE

REAGENT or RESOURCE	SOURCE	IDENTIFIER
Antibodies		
Anti-HERC2 antibody	Abcam	Cat. # Ab85832
Anti-Flag antibody	Sigma-Aldrich	Cat. # F3165
Anti-GST antibody	Santa Cruz	Cat. # sc-459
Bacterial and Virus Strains		
Escherichia coli BL21-CodonPlus (De3) RIL	Agilent Technologies	N/A
Chemicals, Peptides, and Recombinant Proteins		
Dithiothreitol	Gold Biotechnology	27565-41-9
β-mercaptoethanol	Sigma-Aldrich	Cat. # M6250
Phenylmethanesulfonyl fluoride	Sigma-Aldrich	Cat. # P7626
$^{15}NH_4Cl$	Sigma-Aldrich	Cat. # 299251
IPTG	Gold biotechnology	Cat. # I2481
Ni-NTA beads	QIAGEN	Cat. # 30210
Glutathione Sepharose 4B beads	GE Healthcare	Cat. # 17-0756-01
Streptavidin magnetic beads	Thermo Fisher Sci	Cat. # 88816
ANTI-FLAG M2 Magnetic Beads	Sigma-Aldrich	Cat. # A2220
$H3_{1-12}$, $SUMO1_{1-6}$ peptides	Synpeptide	N/A
$H3_{1-22}$, $H4_{1-24}$, $H2A_{1-22}$, $H2B_{1-22}$ peptides	Synpeptide	N/A
Modified $H3_{1-22}$ peptides	Synpeptide	N/A
TEV and Ulp1 proteases	Home expressed	N/A
Deposited Data		
Crystal structure of $SUMO1_{1-6}$ linked $HERC2_{ZZ}$	This study	PDB: 6WW3
Crystal structure of $H3_{1-6}$ linked $HERC2_{ZZ}$	This study	PDB: 6WW4
Crystal structure of p300 ZZ domain in complex with histone H3 peptide	Zhang et al., 2018b	PDB: 6DS6
Experimental Models: Cell Lines		
Human: HEK293T	ATCC	Cat. # CRL-3216
Oligonucleotides		
All primer oligonucleotides are reported in Table S1	This study - IDT	N/A
Recombinant DNA		
Plasmid: pDEST15	Thermo Fisher Sci	Cat. # 1180214
Plasmid: pCIOX	Andrea Mattevi lab, University of Pavia	Addgene, Cat. # 51300
Software and Algorithms		
HKL2000	Otwinowski and Minor, 1997	https://www.hkl-xray.com/download-instructions-hkl-2000
Phenix	Adams et al., 2010	http://www.phenix-online.org/
Coot	Emsley et al., 2010	https://www2.mrc-lmb.cam.ac.uk/personal/pemsley/coot/

REAGENT or RESOURCE	SOURCE	IDENTIFIER
KaleidaGraph 4.5	Synergy Software	https://www.synergy.com/

Table 1.

Data Collection and Refinement Statics for the $HERC2_{ZZ}$:$H3_{1-6}$ and $HERC2_{ZZ}$:$SUMO1_{1-6}$ Complexes

	$H3_{1-6}$-$HERC2_{ZZ}$	**$SUMO1_{1-6}$-$HERC2_{ZZ}$**
PDB	**6WW4**	**6WW3**
Data Collection		
Space group	$P2_1$	$P2_12_12_1$
Cell dimensions		
a, b, c (Å)	24.93, 76.44, 33.01	41.88, 47.26, 55.48
α, β, γ (°)	90.00, 102.52, 90.00	90.00, 90.00, 90.00
Wavelength (Å)	1.28	1.54
Resolution[a] (Å)	38.23–2.25 (2.33–2.25)	33.43–2.10 (2.18–2.10)
Completeness (%)	91.0 (54.7)	98.2 (99.8)
Redundancy	5.9 (3.2)	4.2 (4.3)
CC½ in highest shell	0.963	0.900
R_{sym} or R_{merge} (%)	8.3 (15.7)	16.4 (34.9)
I/σI	16.2 (5.7)	8.3 (3.8)
Refinement		
Resolution (Å)	38.22–2.25	33.43–2.10
Unique reflections	5,256	6,735
R_{work}/R_{free}	19.85/24.34	18.47/22.68
Root-mean-square deviation		
Bond lengths (Å)	0.007	0.008
Bond angles (°)	0.850	0.961
B factors (Å^2)		
Protein	29.51	13.63
Zn	35.59	11.65
Water	31.15	20.84
No. of atoms		
Protein	904	945
Zn	4	4
Water	53	129
Ramachandran plot (%)		
Favored	95.2	97.3
Allowed	4.8	2.7
Outlier	0.0	0.0

[a]Values in parentheses are for highest-resolution shell.